ISSN 1674-1056
http://cpb.iphy.ac.cn
http://iopscience.iop.org/cpb
中国物理 B
Chinese Physics
中国物理
Chinese Physics B

Free-standing, curled and partially reduced graphene oxide network as sulfur host for high-performance lithium-sulfur batteries

Hui-Liang Chen(陈辉亮), Zhuo-Jian Xiao(肖卓建), Nan Zhang(张楠), Shi-Qi Xiao(肖仕奇), Xiao-Gang Xia(夏晓刚), Wei Xi(席薇), Yan-Chun Wang(王艳春), Wei-Ya Zhou(周维亚), Si-Shen Xie(解思深)
Citation: Chin. Phys. B . 2018, 27(6): 068101. **doi:** 10.1088/1674-1056/27/6/068101

Journal homepage: http://cpb.iphy.ac.cn; http://iopscience.iop.org/cpb

What follows is a list of articles you may be interested in

Thermal conduction of one-dimensional carbon nanomaterials and nanoarchitectures

Haifei Zhan(占海飞), Yuantong Gu(顾元通)
Chin. Phys. B . 2018, 27(3): 038103. **doi:** 10.1088/1674-1056/27/3/038103

Electromechanical actuation of CNT/PVDF composite films based on a bridge configuration

Xiaogang Gu(谷孝刚), Xiaogang Xia(夏小刚), Nan Zhang(张楠), Zhuojian Xiao(肖卓建), Qingxia Fan(范庆霞), Feng Yang(杨丰), Shiqi Xiao(肖仕奇), Huiliang Chen(陈辉亮), Weiya Zhou(周维亚), Sishen Xie(解思深)
Chin. Phys. B . 2017, 26(7): 078101. **doi:** 10.1088/1674-1056/26/7/078101

Carbon-nanodot-coverage-dependent photocatalytic performance of carbon nanodot/TiO_2nanocomposites under visible light

Ming-Ye Sun(孙明烨), You-Jin Zheng(郑友进), Lei Zhang(张蕾), Li-Ping Zhao(赵立萍), Bing Zhang(张冰)
Chin. Phys. B . 2017, 26(5): 058101. **doi:** 10.1088/1674-1056/26/5/058101

Rare earth Ce-modified (Ti,Ce)/a-C: H carbon-based filmon WC cemented carbide substrate

Shengguo Zhou(周升国), Zhengbing Liu(刘正兵), Shuncai Wang(王顺才)
Chin. Phys. B . 2017, 26(1): 018101. **doi:** 10.1088/1674-1056/26/1/018101

Tunable thermoelectric properties in bended graphene nanoribbons

Chang-Ning Pan(潘长宁), Jun He(何军), Mao-Fa Fang(方卯发)
Chin. Phys. B . 2016, 25(7): 078102. **doi:** 10.1088/1674-1056/25/7/078102

Free-standing, curled and partially reduced graphene oxide network as sulfur host for high-performance lithium–sulfur batteries*

Hui-Liang Chen(陈辉亮)[1,2,3], Zhuo-Jian Xiao(肖卓建)[1,2,3], Nan Zhang(张楠)[1,2,3], Shi-Qi Xiao(肖仕奇)[1,2,3], Xiao-Gang Xia(夏晓刚)[1,2,3], Wei Xi(席薇)[1,2,3], Yan-Chun Wang(王艳春)[1,2], Wei-Ya Zhou(周维亚)[1,2,3,†], and Si-Shen Xie(解思深)[1,2,3,‡]

[1] *Beijing National Laboratory for Condensed Matter Physics, Institute of Physics, Chinese Academy of Sciences, Beijing* 100190, *China*
[2] *Beijing Key Laboratory for Advanced Functional Materials and Structure Research, Beijing* 100190, *China*
[3] *School of Physical Sciences, University of Chinese Academy of Sciences, Beijing* 100049, *China*

(Received 3 April 2018; revised manuscript received 27 April 2018; published online 30 May 2018)

Lithium–sulfur (Li–S) batteries have received more and more attention because of higher specific capacity and energy density of sulfur than current lithium–ion batteries. However, the low electrical conductivity of sulfur and its discharge product, and also the high dissolution of polysulfides restrict the Li–S battery practical applications. To improve their performances, in this work, we fabricate a novel free-standing, curled and partially reduced graphene oxide (CPrGO for short) network and combine it with sulfur to form a CPrGO–S composite as a cathode for Li–S battery. With sulfur content of 60 wt%, the free-standing CPrGO–S composite network delievers an initial capacity of 988.9 mAh·g^{-1}. After 200 cycles, it shows a stable capacity of 841.4 mAh·g^{-1} at 0.2 C, retaining about 85% of the initial value. The high electrochemical performance demonstrates that the CPrGO–S network has great potential applications in energy storage system. Such improved properties can be ascribed to the unique free-standing and continous CPrGO–S network which has high specific surface area and good electrical conductivity. In addition, oxygen-containing groups on the partially reduced graphene oxide are beneficial to preventing the polysulfides from dissolving into electrolyte and can mitigate the "shuttle effect".

Keywords: lithium–sulfur batteries, sulfur cathode, curled reduced graphene oxide

PACS: 81.05.U–, 88.80.ff, 81.05.ue **DOI:** 10.1088/1674-1056/27/6/068101

1. Introduction

With the increasing demand of sustainable and clean energy storage, especially in the portable electronic devices and electric vehicles markets, traditional lithium–ion (Li-ion) batteries based on conventional insertion compounds have encountered their bottlenecks because of the limited theoretic specific capacity.[1] Recently, lithium–sulfur (Li–S) batteries have received significant attention because their high theoretical specific capacity of 1672 mAh·g^{-1} and specific energy density 2567 W·h·kg^{-1} based on the electrochemical reaction of $S_8+16Li^++16e^{-1}\rightarrow 8Li_2$ S, which is more than five times that of Li-ion batteries. For now, Li–S batteries have been greatly considered as one of the most promising next-generation energy storage systems.[2,3] In addition, elemental sulfur has other advantages, such as its natural abundance, low cost, and less environmental pollution.[4]

However, the commercialisation of Li–S batteries is hindered to a great extent by their fast capacity fading, poor rate-performance, and low sulfur utilization. These major problems can be ascribed to the following critical issues:[1,5,6] (i) the low electrical conductivity of sulfur and its solid-state discharge product (Li_2S); (ii) the high dissolution of intermediate polysulfides and gradual loss of active sulfur from the cathode into electrolyte and onto the Li metal anode, which are known as "shuttle effect"; (iii) the large volumetric expansion (over 80%) from sulfur to Li_2S after lithiation, inducing the mechanical damage of cathode.

To address the problems mentioned above, a lot of efforts have devoted to enhancing the electrical conductivity and preventing polysulfides from dissolving. Various kinds of composites have been fabricated by the combination of sulfur and conductive materials, such as porous carbon,[3,7] graphene,[8–11] carbon nanotubes,[12–14] and conductive polymers.[15,16] Among these materials, graphene is considered as one of the most promising conductive materials because of its high electrical conductivity, superior mechanical flexibility, high chemical and thermal stability, and large specific surface area.[11,17–19] Moreover, reduction of graphene oxide (GO) prepared by the modified Hummers method provides a way to produce graphene on a large scale for practical applications.[20] However, because graphene layers tend to agglomerate, many unique properties of graphene are unavailable.[21] In order to make the best graphene in property, many excellent composite structures of graphene with

*Project supported by the National Basic Research Program of China (Grant No. 2012CB932302), the National Natural Science Foundation of China (Grant Nos. 11634014, 51172271, and 51372269), and the Strategic Priority Research Program of the Chinese Academy of Sciences (Grant No. XDA09040202).

†Corresponding author. E-mail: wyzhou@iphy.ac.cn
‡Corresponding author. E-mail: ssxie@iphy.ac.cn

© 2018 Chinese Physical Society and IOP Publishing Ltd

sulfur were reported,[8,19,22] Cui *et al.* coated GO on sulfur particles and the core–shell structure showed an initial capacity of $\sim$ 750 mAh·g^{-1}, followed by a decrease to a capacity of $\sim$ 600 mAh·g^{-1} at 0.2 C (1 C = 1672 mA·g^{-1}) over more than 100 cycles. It is noted that most of the graphene–sulfur composites were prepared primarily on a conventional doctor-blade casting method.[8,9,19] But the method introduces the conductive binders and metal current collector, thereby increasing the cathode weight and unavoidably dilute the gravimetric energy density. Therefore, it is necessary to develop binder-free graphene–sulfur composites for Li–S batteries.[11,23] Cheng's group constructed fibrous hybrid rGO–S materials by the hydrothermal method and obtained 550 mAh·g^{-1} at 0.45 C after 100 cycles with a retention of 78%.[11] So far, although substantial progress based on GO system has been made in recent years, it is still a great challenge to achieve the robust cycling performance while to keep high specific capacity and energy density.

In this study, we improve a synthesis approach and successfully fabricate a free-standing, curled and partially reduced graphene oxide (CPrGO) network, which can be directly used as a sulfur host material to prepare the cathode of Li–S battery. When assembled into a cell, the as-obtained composite network of CPrGO and S (CPrGO–S) shows an outstanding cycling stablility with high specific capacity. The excellent performance can be put down to the synergistic effect from the good conductive porous network with high specific surface area and the oxygen-containing functional groups on CPrGO surfaces. This effect can not only facilitate the infiltration of electrolyte and transformation of lithium ions, but also prevent the polysulfide from dissolving by strong binding between the oxygen-containing groups and polysulfides. In addition, the free-standing CPrGO–S compoiste electrode avoids using the conductive binders and metal current collectors, and therefore has a large overall capacity.

2. Experimental section

2.1. Preparation of CPrGO–S composite

2.1.1. Preparation of GO aqueous solution

GO was synthesized by modified Hummers method. 3 g of graphite powder, 1.5 g of $NaNO_3$ and 70 mL of concentrated H_2SO_4 were mixed in an ice–water bath under magnetic stirring. 9 g of $KMnO_4$ was gradually added to the above mixture while keeping the temperature at 40 °C for 3 h. Deionized water (140 mL) was slowly dropped into the resulting solution followed by another 200 mL of deionized water. Then 20 mL of H_2O_2 (30 wt%) was slowly added and stirred for 10 min to obtain GO suspensions. The brown mixed solution was rinsed with deionized water using a centrifuge system several times. Finally, the GO aqueous solution was obtained.

2.1.2. Preparation of CPrGO network

5-mL aqueous dispersion of GO (0.5 mg·mL^{-1}) and 5 mL of glucose solution (0.5 mg·mL^{-1}) were mixed and stirred to disperse and finally formed a stable dispersion solution. After the infusion of prepared solution into the cylindrical mold made by PTFE, we used liquid nitrogen to freeze the PTFE mold until all the solution was frozen. Then lyophilization was carried out by the vacuum-freeze-drying apparatus to remove water. Thus, a stable and intact sample of porous GO network with glucose (GO-g for short) was obtained with the same shape as the mold. For convenience in assembling into button cell, we specially designed the PFTE mold size on the basis of CR2032.

The GO foam without the addition of glucose was prepared by the same procedure with GO-g network.

The as-obtained GO-g network was heated at 180 °C for at least 12 h. To remove excess glucose, the GO-g network was washed many times by immerging into the mixed solution of deionized water and ethanol at 60 °C. Finally, the pure CPrGO network was achieved by drying process.

2.1.3. Preparation of CPrGO–S composite

Porous CPrGO–S composite was prepared by a melt-diffusion approach. Briefly, the pure CPrGO network and sulfur, at the weight ratios of 5:5, 4:6, and 3:7, were co-heated to 155 °C for 12 h in an autoclave under argon atmosphere, respectively.

2.1.4. Preparation of PrGO–S film

Partially reduced graphene oxide (PrGO) film was obtained by vacuum filtration of GO aqueous solution and subsequent heat treatment at 180 °C for 12 h. Then, by the melt-diffusion approach, a PrGO–S film was fabricated. Its mass per unit area was the same as that of CPrGO–S composite.

2.2. Material characterization

Morphologies of the samples were characterized by field-emission scanning electron microscopy (SEM) using S-4800 (Hitachi, Japan) equipped with energy disperse spectroscopy (EDS, EMAX 7593-H, HORIBA). Raman spectra were recorded with the laser of 514 nm (Lab RAM HR800, HORIBA Jobin Yvon Inc.). X-ray diffraction (XRD) measurements (D8 Advance, Bruker) were performed with Cu Kα radiation. Fourier-transformed infrared (FTIR) spectra were recorded on a Bruker VERTEX 70v spectrometer. The ratio of sulfur was obtained by weighting the change of mass before and after adding sulfur using XP2U ultramicro balance (Mettler toledo, Switzerland).

2.3. Cell assembly and electrochemical measurement

A free-standing CPrGO–S network with a diameter of 10 mm was directly used as the cathode of Li–S battery.

CR2032-type coin cells were assembled in an argon-filled glove box (MBraun, Unilab) with lithium foil as the counter electrode. The electrolyte was 1.0-M lithium bis-trifluoromethane sulfonyl-imide (LiTFSl) and 2-wt% lithium nitrate ($LiNO_3$) in 1,3-dioxolane (DOL) and 1,2-dimethoxyethane (DME) (1:1 by volume ratio). A Celgard 2400 polypropylene membrane was used as the separator. The PrGO–S film was cut into disk with a diameter of 10 mm and was also assembled as a cathode in the same way as the above. The galvanostatic chargedischarge test with a potential window of 1.7 V–2.8 V (versus Li^+/Li) was performed by a Land CT-2001 A (Wuhan, China) battery analyser. The cyclic voltammetry (CV) and electrochemical impedance spectroscopy (EIS) were conducted on an electrochemical workstation (IM6, Zahner). During the measurements, CV was performed at a scanning rate of 0.1 $mV{\cdot}s^{-1}$ in the potential window of 1.5 V–3.0 V. EIS was carried out at open circuit potential and the potentiostatic signal amplitudes of 5 mV in the frequency range from 0.1 Hz to 100 kHz. Unless otherwise specified, all experiments were conducted at room temperature and the characterizations were based on CPrGO–S composites with sulfur loading of 60 wt%. Moreover, all the specific capacities were calculated based on sulfur mass in the electrodes.

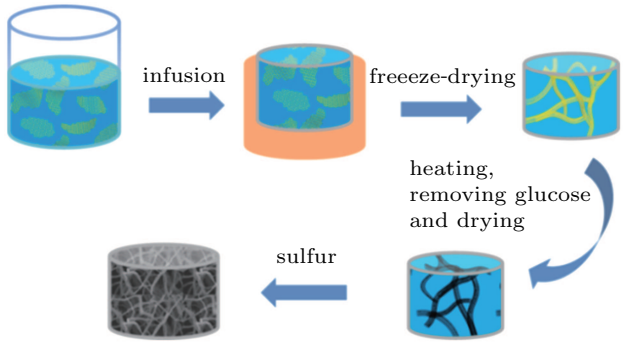


Fig. 1. (color online) Schematic illustration of the fabrication process of a free-standing CPrGO–S composite network.

3. Results and discussion

Schematic illustration of the fabrication process of a free-standing CPrGO–S network is shown in Fig. 1. Its free-standing feature originates from the GO-g network in the freeze-drying process and preserves over subsequent procedures. A stable, intact and porous GO-g sample with the same shape as the mold is demonstrated in Fig. S1(a), which indicates that it is self supporting.

As can be seen in Figs. 2(a) and 2(c), the CPrGO displays interconnected network. It is worth mentioning that different CPrGO layers, with a width of about 1 μm (see Appendix A in Fig. S2(a)), are entangled with each other and their overlapped parts have good contacts by Y-type junctions (Fig. S2(b)), which build a continuous network with good electrical conductivity. Moreover, the free-standing network displays a distribution of pores in several micrometer ranges. The above features are maintained very well in the CPrGO–S composites (Figs. 2(b) and 2(d)) prepared by the combination of CPrGO network with sulfur *via* melt-diffusion approach. The homogeneous carbon and sulfur mapping in the same region of Fig. 2(b) as shown in Figs. 2(e) and 2(f), respectively, confirm the uniform distribution of sulfur in the composite. These features can largely enhance the permeation of electrolyte, diffusion of lithium ions as well as accommodation of the large volume effect. It is noted that even after charge-discharge 200 times, the CPrGO–S composite still keeps an original morphology (Fig. S3 in Appendix A), which further demonstrates its robust structure.

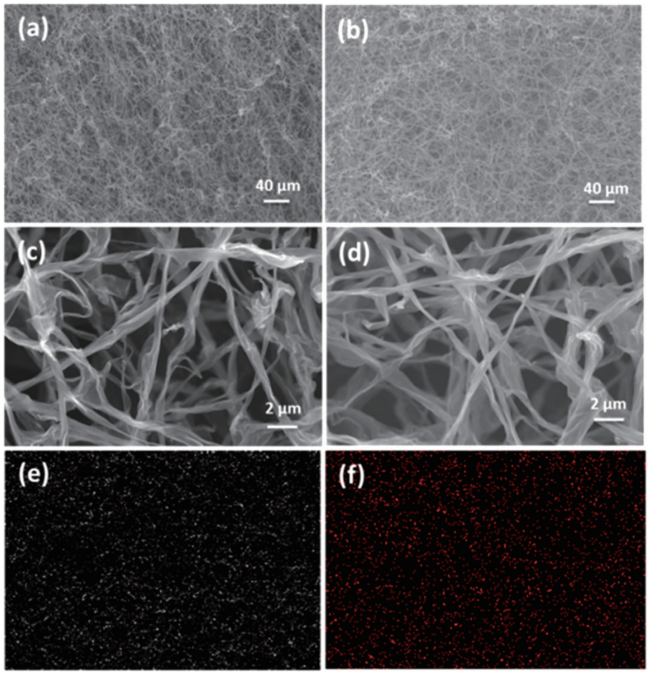


Fig. 2. SEM images of ((a), (c)) CPrGO and ((b), (d)) CPrGO–S at different magnifications. (e) carbon and (f) sulfur mapping of the region in panel (b).

At high magnification image of a CPrGO–S network, as illustrated in Fig. S2(a), the layers form curled shapes (marked by white arrows) connected by many Y-junctions, which will restrict the stacking of graphene layers and highly increase the surface area. Its microstructure duplicates the CPrGO networks, but contrasts with the PrGO foam without the addition of glucose. The latter exhibits disorder and dispersive flaky layers shown in Figs. S4(a) and S4(b), which account for the loose macroscopic morphology. A PrGO film, prepared by vacuum filtrations, manifests a dense surface without evident pores (Figs. S4(c) and S4(d)). It indicates severe stacking of graphene layers in the process of filtration. The reason why graphene layers formed interconnected curled graphene with the addition of glucose may be due to the connection function of glucose among graphene layers and the specific temperature gradient field. The detailed mechanism needs further studying.

Raman spectra of different samples (GO foam, CPrGO and CPrGO–S networks) are shown in Fig. 3(a). Although the relevant peaks are slightly changed in shape and shifted a

little, they are located at around 1355 cm^{-1} and 1597 cm^{-1}, which are identified as the D band (disorder-induced phonon mode) and the G band (graphite band) of graphene nanosheets. The intensity ratios of I_D/I_G based on the relevant peaks are calculated to be 0.40, 0.89, and 0.90 for GO foam, CPrGO and CPrGO–S networks, respectively. Therefore, after the introduction of sulfur, CPrGO–S composite can keep the same I_D/I_G as that of CPrGO network, but they both have more defects than GO foam. Their larger ratios would correspond to the increase of edges and the unrepaired defects introduced in partial reduction treatment of GO, which is consistent with previous studies.[24,25]

FTIR spectra of CPrGO and CPrGO–S networks are shown in Fig. 3(b). It can be seen that the strong and broad absorption at 3380 cm^{-1} is attributed to O–H stretch vibration. The peaks at 1650, 1400, and 1050 cm^{-1} are ascribed to carboxyl O = C–O bonds, C–OH bonds and alkoxy C–O bonds, respectively.[26,27] In comparison with GO foam, most of these oxygen-functional groups are significantly reduced, and the peaks at 1570 cm^{-1} and 1220 cm^{-1}, due to C = C and epoxy C–O, become dominant in both CPrGO and CPrGO–S networks. This proves that the GO has been partially reduced to graphene during heat treatment at 180 °C. It is worth mentioning that the major oxygen-containing functional groups remaining in CPrGO and CPrGO–S networks are epoxy/hydroxy groups,[11,28] which would benefit their electrochemical performance.

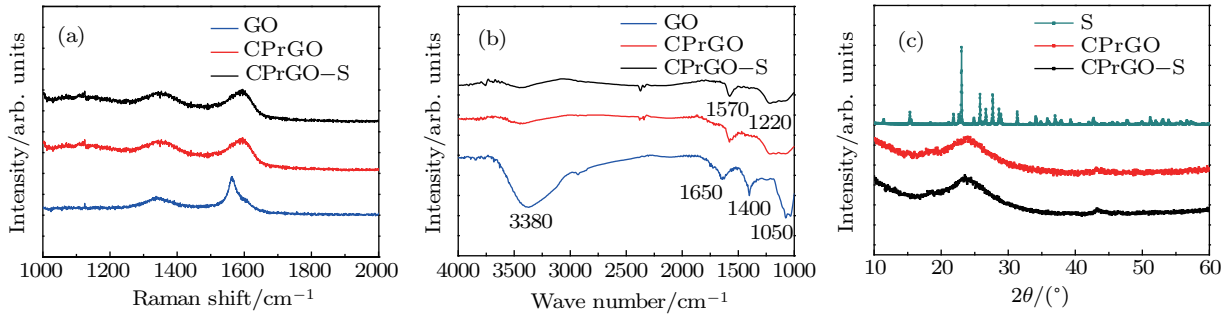


Fig. 3. (color online) (a) FT-IR spectra and (b) Raman spectra of GO foam, CPrGO, and CPrGO–S networks. (c) XRD patterns of pure sulfur powder, CPrGO and CPrGO–S networks.

The detailed structure and composition of pure sulfur powder, CPrGO and CPrGO–S networks are analysed by XRD. Figure 3(c) shows that sulfur exhibits very sharp and strong peaks throughout the entire diffraction range, indicating a well-defined crystal S_8 structure. In contrast with pure sulfur, no obvious characteristic peaks of sulfur can be observed for the CPrGO–S composite. Only one broad peak centered at 24° is found in CPrGO and CPrGO–S networks, which suggests that the sulfur is amorphous in the CPrGO–S network.[29] In addition, no new peak found in CPrGO–S composite proves that no new phase is generated in the fabrication process.

To demonstrate the microstructural advantages of CPrGO–S network, systematical electrochemical measurements are performed. The electrochemical route to the CPrGO–S composite material is monitored by cyclic voltammetry analysis for the initial three cycles between 1.5 V and 3.0 V as shown in Fig. 4(a). In the first cycle, two cathodic peaks are observed at 1.97 and 2.20 V due to the multistep reduction of elemental sulfur with lithium. Specifically, the peak at 2.20 V is attributed to the reduction of S_8 molecules to high-order polysulfides (Li_2S_n, $4 < n <= 8$),[30] while the peak at 1.97 V is associated with the further reduction of soluble high-order polysulfides to loworder polysulfides (such as Li_2S_4, Li_2S_3, and Li_2S_2) and Li_2S,[31,32] in which Li_2S_2 and Li_2S are insoluble. In the subsequent anodic scan, the only one anodic peak at 2.48 V is assigned to the coupled conversion from Li_2S to polysulfides (Li_2S_n, $1 < n <= 8$), and ultimately to elemental sulfur. These results are in agreement with galvanostatic charge-discharge curves (Fig. 4(b)) and similar to other reports.[8,33,34] From the second cycle, both the peak positions and areas undergo very little change, suggesting high electrode stability and hence, good capacity retention.

Figure 4(b) shows galvanostatic charge-discharge curves of the CPrGO–S composite at a current rate of 0.2 C. It is obvious that the charge–discharge plateaus resemble the redox peaks observed in cyclic voltammetric scan. In brief, two typical plateaus behaviors are ascribed to the formation of high-order lithium polysulfides and low-order lithium sulfides in the discharge process.[11,35,36] The CPrGO–S composite assembled into coin cell, acting as a cathode, delivers an initial capacity of 988.9 $mAh{\cdot}g^{-1}$ at 0.2 C (Fig. 4(c)), and the overall capacity of the cathode (including sulfur and CPrGO) is 593.3 $mAh{\cdot}g^{-1}$, calculated according to the known sulfur weight ratio. The capacity can be maintained at 841.4 $mAh{\cdot}g^{-1}$ after 200 cycles, which exhibits a stable capacity retention of over 85%, with capacity loss 0.075% per cycle. It is worth noting that the cathode shows a capacity fading and then a capacity increasing within the first 45 cycles. The capacity fading at the beginning of cycling may be associated with the poor electrochemical contact in the original sulfur electrode, resulting in the low sulfur utilization.[37,38] Then the capacity gradually increases with the improvement

of chemical activity of sulfur due to the redistribution of active sulfur in the charge process.[37] After 45 cycles, the capacity displays a less fading rate of 0.029% per cycle, suggesting that the outward migration of dissolved polysulfides and loss of active sulfur are greatly suppressed by the strong interaction between sulfur/polysulfides and graphene surface.[9,11,31] Furthermore, the Coulombic efficiency is above 98% for all CPrGO–S composites with different sulfur ratios during cycling (Figs. 4(c) and S5), indicating that the shuttling effect is effectively avoided in the Li–S batteries.

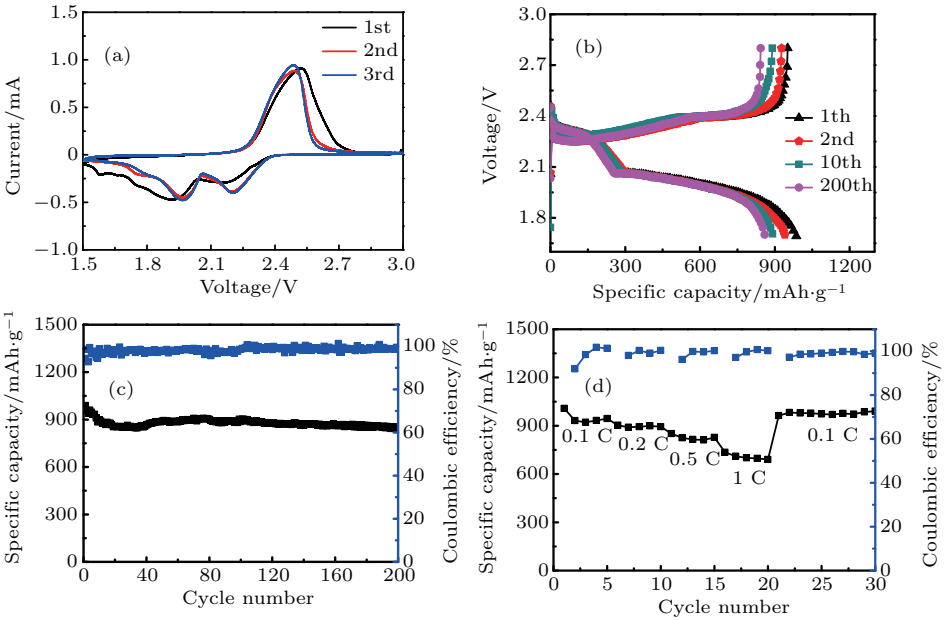


Fig. 4. (color online) (a) CV profiles of CPrGO–S composite cathode at a scan rate of 0.1 mV·s^{-1}. (b) Galvanostatic charge–discharge curves of CPrGO–S network. (c) Cycling performance at 0.2 C for 200 cycles. (d) Rate performances at various current densities of CPrGO–S network.

The PrGO filtration film (Fig. S6(a)) possesses an initial specific capacity of 897.6 mAh·g^{-1}. After 100 cycles, the capacity decreases to 409.7 mAh·g^{-1}, showing a large capacity decay of 54%. What is more, the capacity still has obvious downward trend, reflecting the poor cycling performance. In comparison with CPrGO network, the PrGO filtration film equally contains oxygen groups which can bind the polysulfides and restrain their dissolution into electrolyte in the same way, but its dense stacked layers seriously hinder the infusion of electrolyte and diffusion of lithium ions, leading to the rapid fading of capacity.

The rate capacity of CPrGO–S network electrode is illustrated in Fig. 4(d). The CPrGO–S network delivers a high initial specific capacity of 1007.3 mAh·g^{-1} at a current density of 0.1 C. With current density increasing to 0.2 C, 0.5 C, and 1 C, the corresponding discharge specific capacities are 890, 815, and 700 mAh·g^{-1} with the overall capacities of the cathode being 534, 489, and 420 mAh·g^{-1}, displaying a gradually decreasing trend. When the cycling current is restored to 0.1 C, a discharge capacity of 960 mAh·g^{-1} can be well recovered, implying the stable structure, low polarization and the high reversibility of the cathode. Compared with PrGO filtration film (Fig. S6(b)), the CPrGO–S network exhibits much high capacities at different current densities ranging from 0.1 C to 1 C. The superior rate performance of CPrGO–S network further indicates that the unique architecture significantly enhances the electrochemical stability of the composite cathode.

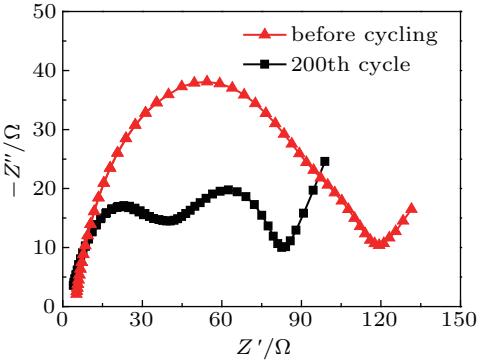


Fig. 5. (color online) Nyquist plots of CPrGO–S network before and after cycling.

The EIS tests of CPrGO–S before and after cycling are conducted. As shown in Fig. 5, the Nyquist plot of battery after 200 cycles consists of two depressed semicircles and a short line. Specifically, the semicircle at high frequency is considered as being due to the resistance of the accumulated lithium sulfide interlayer formed on the surface of the lithium anode, suggesting the dissolution of polysulfides followed by their deposition on the electrode to form passivation films. The semicircle in middle frequency region, which only the plot of battery before cycling has, corresponds to charge-transfer resistance (R_{ct}). The positive slope at low frequency is related to Warburg impedance, due to the diffusion process of lithium ions in the active material of the electrode.[23] As shown in Fig. 5, It can be found that R_{ct} decreases from about 100 Ω to 40 Ω after 200 cycles. It indicates that there are closer contacts between the sulfur and CPrGO networks because of the rear-

rangement of the physically stable sulfur occupying a more electrochemically favorable position.[39]

4. Conclusions

We have designed and fabricated a free-standing CPrGO–S network by the combination of CPrGO with sulfur. The CPrGO–S composite possesses a continuous porous structure with curled morphology as well as good conductivity, which facilitates the infiltration of electrolyte and transportation of lithium ions. The oxygen-containing functional groups on the CPrGO surface can efficiently improve the utilization of sulfur and cycling performance by binding lithium polysulfides. Moreover, the CPrGO–S networks can be directly assembled into cathodes without metal current-collectors and conductive binders. When cycling at 0.2 C, the composite electrode delivers a high initial capacity of 988.8 mAh·g^{-1} and an excellent cycling stability for 200 cycles with a capacity retention of 85%. What is more, after 45 cycles, the specific capacity shows slight decrease with the fading rate of only 0.029% per cycle. The excellent results demonstrate that the free-standing CPrGO–S composite networks can be promising cathodes for long-life Li–S batteries, and also have great potential applications in high energy density flexible power devices. In addition, the fabrication of CPrGO also opens up fresh perspectives of using graphene as free-standing porous materials for wide applications, such as lithium-air batteries, supercapacitors and catalyses.

Appendix A. Supporting information

Some supporting materials for better understanding this paper are provided in the following figures.

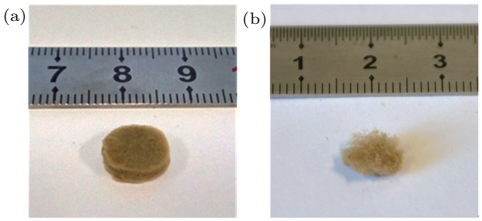


Fig. S1. (color online) Optical photographs of (a) GO-g network and (b) GO foam after freeze-drying. The former is stable and intact with the same shape as the mold. However, the latter is very easy to fall apart and often to be blown away by slight airflow. So, it fails to form a stable free-standing foam, nor does it carry out the follow-up processes either.

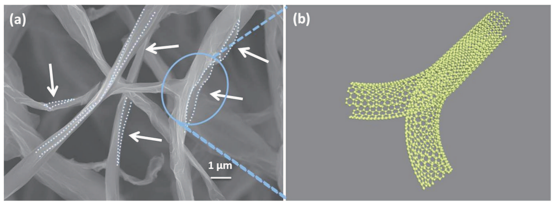


Fig. S2. (color online) (a) SEM image of CPrGO network and (b) corresponding schematic illustration of a curled shape connected by Y-junction. Area marked by blue ellipse shows that different rGO layers intertwine to form Y-type junction, which can improve electrical conductibility and facilitate the formation of a free-standing continuous network. Areas marked by white arrows illustrate that layers form curled shapes, which would restrict the stacking of graphene layers and increase surface area.

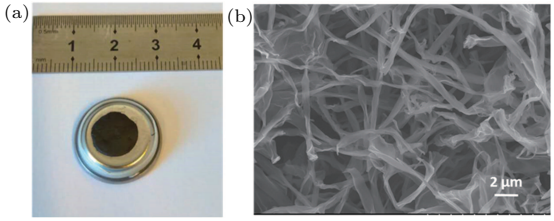


Fig. S3. (color online) (a) Optical photograph and (b) SEM image of CPrGO–S composite after cycling. To investigate structural stability of CPrGO–S composite, after discharging and charging circulation at 0.2 C 200 times, the cell is disassembled and the CPrGO–S composite is rinsed to remove electrolytes. It is demonstrated that CPrGO–S composite can still keep integrity with free-standing after cycling. Moreover, its microstructure also remains interconnected network with curled morphology.

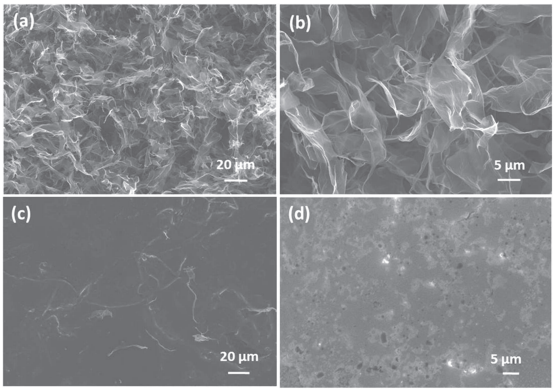


Fig. S4. SEM images with different magnifications of ((a), (b)) PrGO foam without the addition of glucose and ((c), (d)) PrGO filtration film. The PrGO without the addition of glucose is obtained by further heat treatment of sample as shown in Fig. S1(b). To fabricate PrGO filtration film, we first perform vacuum filtration to obtain GO film of the same mass per unit area as freeze-drying GO foam, then heated the GO film at 180 °C for 12 h.

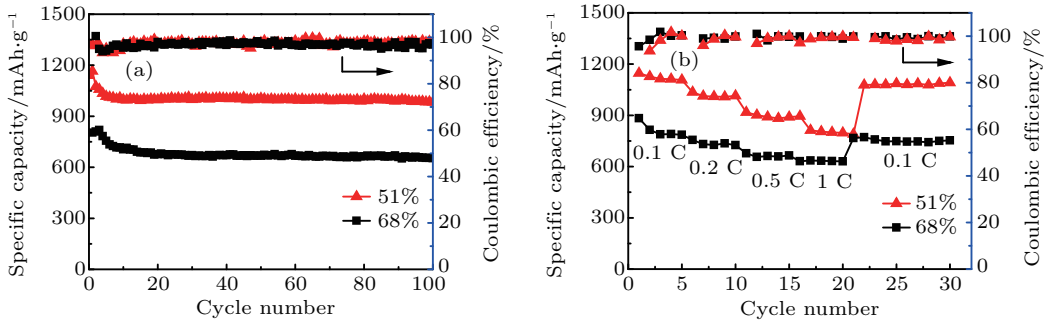


Fig. S5. (color online) (a) Cycling stability at 0.2 C and (b) rate performance of CPrGO–S composite networks with sulfur loading of 51 wt% and 68 wt%. It is noted that two composites and other one in text (60-wt% sulfur loading) have the same mass per unit area as that of the basic CPrGO networks.

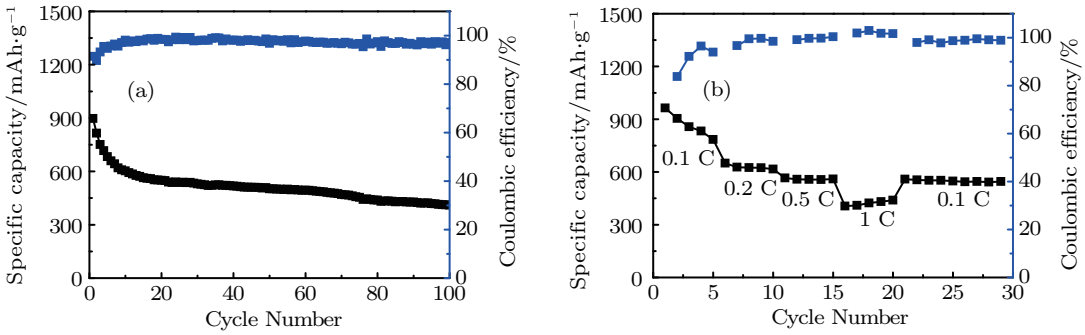


Fig. S6. (color online) (a) Cycling stability at 0.2 C and (b) rate performance of PrGO filtration film with 60 wt% sulfur. To prepare the cathode, the PrGO–S film is cut into disc with a diameter of 10 mm, and the whole weight of film is the same as that of CPrGO–S network (60-wt% sulfur loading).

References

[1] Ji X L and Nazar L F 2010 *J. Mater. Chem.* **20** 9821
[2] Bruce P G, Freunberger S A, Hardwick L J and Tarascon J M 2012 *Nat. Mater.* **11** 19
[3] Ji X, Lee K T and Nazar L F 2009 *Nat. Mater.* **8** 500
[4] Yin Y X, Yao H R and Guo Y G 2016 *Chin. Phys. B* **25** 018801
[5] Scrosati B, Hassoun J and Sun Y K 2011 *Energy Environ. Sci.* **4** 3287
[6] Wang J, He Y S and Yang J 2015 *Adv. Mater.* **27** 569
[7] Schuster J, He G, Mandlmeier B, Yim T, Lee K T, Bein T and Nazar L F 2012 *Angew. Chem. Int. Ed.* **51** 3591
[8] Wang H, Yang Y, Liang Y, Robinson J T, Li Y, Jackson A, Cui Y and Dai H 2011 *Nano Lett.* **11** 2644
[9] Rong J, Ge M, Fang X and Zhou C 2014 *Nano Lett.* **14** 473
[10] Liang Z, Liwen J, Glans P A, Yuegang Z, Junfa Z and Jinghua G 2012 *PCCP* **14** 13670
[11] Zhou G, Yin L C, Wang D W, Li L, Pei S, Gentle I R, Li F and Cheng H-M 2013 *Acs Nano* **7** 5367
[12] Sun L, Li M, Jiang Y, Kong W, Jiang K, Wang J and Fan S 2014 *Nano Lett.* **14** 4044
[13] Zhao M Q, Liu X F, Zhang Q, Tian G L, Huang J Q, Zhu W C and Wei F 2012 *Acs Nano* **6** 10759
[14] Peng H J, Huang J Q, Zhao M Q, Zhang Q, Cheng X B, Liu X Y, Qian W Z and Wei F 2014 *Adv. Funct. Mater.* **24** 2772
[15] Ma G, Wen Z, Jin J, Lu Y, Wu X, Wu M and Chen C 2014 *J. Mater. Chem. A* **2** 10350
[16] Wu F, Chen J Z, Chen R J, Wu S X, Li L, Chen S and Zhao T 2011 *J. Mater. Chem. C* **115** 6057
[17] Bai H, Li C and Shi G 2011 *Adv. Mater.* **23** 1089
[18] Wu H, Huang Y, Zong M, Fu H and Sun X 2015 *Electrochim. Acta* **163** 24
[19] Yoo S, Lee J, Kim J M, Seong C Y, Seong K D and Piao Y 2016 *J. Electroanal. Chem.* **780** 19
[20] Segal M 2009 *Nat. Nanotechnol.* **4** 611
[21] Yang X, Zhu J, Qiu L and Li D 2011 *Adv. Mater.* **23** 2833
[22] Lu S, Cheng Y, Wu X and Liu J 2013 *Nano Lett.* **13** 2485
[23] Luo S, Yao M, Lei S, Yan P, Wei X, Wang X, Liu L and Niu Z 2017 *Nanoscale* **9** 4646
[24] Zheng C, To J W F, Chao W, Zhenda L, Nan L, Chortos A, Lijia P, Fei W, Yi C and Zhenan B 2014 *Adv. Energy Mater.* **4** 1400207
[25] Ham H, Khai T V, Park N H, So D S, Lee J W, Na H G, Kwon Y J, Cho H Y and Kim H W 2014 *Nanotechnology* **25** 235601
[26] Strankowski M, Włodarczyk D, Piszczyk Łand Strankowska J 2016 *J. Spectrosc.* **2016** 1
[27] Drewniak S, Muzyka R, Stolarczyk A, Pustelny T, Kotyczka-Morańska M and Setkiewicz M 2016 *Sensors* **16** 103
[28] Huang Z D, Zhang B A, Oh S W, Zheng Q B, Lin X Y, Yousefi N and Kim J K 2012 *J. Mater. Chem.* **22** 3591
[29] Zhang J, Dong Z, Wang X, Zhao X, Tu J, Su Q and Du G 2014 *J. Power Sources* **270** 1
[30] Xiao L, Cao Y, Xiao J, Schwenzer B, Engelhard M H, Saraf L V, Nie Z, Exarhos G J and Liu J 2012 *Adv. Mater.* **24** 1176
[31] Ji L, Rao M, Zheng H, Zhang L, Li Y, Duan W, Guo J, Cairns E J and Zhang Y 2011 *J. Am. Chem. Soc.* **133** 18522
[32] Zhou G M, Wang D W, Li F, Hou P X, Yin L C, Liu C, Lu G Q, Gentle I R and Cheng H M 2012 *Energy Environ. Sci.* **5** 8901
[33] Guo J C, Xu Y H and Wang C S 2011 *Nano Lett.* **11** 4288
[34] Zheng G Y, Yang Y, Cha J J, Hong S S and Cui Y 2011 *Nano Lett.* **11** 4462
[35] Wang Z Y, Dong Y F, Li H J, Zhao Z B, Wu H B, Hao C, Liu S H, Qiu J S and Lou X W 2014 *Nat. Commun.* **5** 5002
[36] Zhao M Q, Zhang Q, Huang J Q, Tian G L, Nie J Q, Peng H J and Wei F 2014 *Nat. Commun.* **5** 3410
[37] Xiang M W, Yang L, Zheng Y F, Huang J, Jing P, Wu H, Zhang Y and Liu H 2017 *J. Mater. Chem. A* **5** 18020
[38] Yang J, Chen F, Li C, Bai T, Long B and Zhou X Y 2016 *J. Mater. Chem. A* **4** 14324
[39] Chung S H and Manthiram A 2013 *Electrochim. Acta* **107** 569